Available online at www.sciencedirect.com
SCIENCE DIRECT®
Physics and Chemistry of the Earth 29 (2004) 569–577
PHYSICS and CHEMISTRY of the EARTH
www.elsevier.com/locate/pce

Plasma density-electric field turbulence in the low-latitude ionosphere from the observation on satellites; possible connection with seismicity

O.A. Molchanov [a,*], O.S. Akentieva [b], V.V. Afonin [b], E.A. Mareev [c], E. Fedorov [a]

[a] Russian Academy of Sciences, Institute of Physics of the Earth, RAS, Bolshaya Gruzinskaya 10, Moscow, 123995, Russia
[b] Institute of Space Research, RAS, Moscow, Russia
[c] Institute of Applied Physics, RAS, Nizhny Novgorod, 603600, Russia

Received 30 May 2003; received in revised form 20 July 2003; accepted 15 August 2003

Abstract

Based on plasma density data from the Cosmos-900 satellite we have analyzed the spatial distribution of the ionospheric turbulence in a form k^{-b}, where k is wave number and b is the fractal index. In this case spatial scales ($\sim k^{-1}$) are ranging from 15 to 300 km at the satellite height $h = 450$–500 km. Depending on season, local time and seismic activity the index $\langle b \rangle$ varies in the interval 1.3–1.9. Then we have considered the slope of the spatial distribution for electric field turbulence observed on board the IK-24 satellite ($h = 500$–700 km, scales of several meters). Supposing a simple connection between the power spectrum density of the plasma and the electric field we find $\langle b \rangle = 1.2$–1.7. Remembering that from observation on board the Aureol-3 satellite ([Radio Science 20 (1985) 755]; $h = 500$–700 km, scales 10–300 m) $b = 1.7$–1.9 both for the plasma density and electric field variations, we conclude that the ionospheric turbulence is a unique process in a large interval of scales from hundreds km to several meters and the b-dependence is similar to the classic Kolmogorov's turbulence $b = 5/3$. Intensification of the turbulence near the magnetic equator is definitely connected with the presence of the equatorial density anomaly (EA) but existence of the regular moderate level aside of EA and at the mid-latitude ionosphere invokes a possibility of another energy source, probably atmospheric gravity waves.

1. Introduction

It is known that oscillating plasma density irregularities ($\delta_n = n(\mathbf{r}, t) - n_0$) and fluctuations of electric fields ($\mathbf{e} = \mathbf{E}(\mathbf{r}, t) - \mathbf{E}_0$) exist in the ionosphere (e.g. Kelley, 1989), where n_0 and $\mathbf{E}_0$ are averaged (background) values of the density and electric field respectively. Of course the corresponding fluctuations of the magnetic field appear as well, but they are connected directly with the electric field variation. A variety of density irregularities in the low-latitude ionosphere were observed on the ground using either conventional ionosphere sounding (so-called equatorial F-spread effect), by recording of incoherent radar scattering signals or by scintillation technique (Kelly, 1989; Basu et al., 1981; Fejer and Kelley, 1980; Fejer, 1997). As suggested by Kelley (1985), the space scales (wave number spectrum) of the irregularities can be divided into four distinctive wavelength regimes: long (space scale $L \geqslant 20$ km), intermediate ($L = 20$–100 km), transitional ($L = 100$–10 m), and short (L from 10 m up to 0.1 m). There are evidences of similar F-spread phenomena in the mid-latitude area. A review of results using ionosonde observations can be found, for example, in the paper by Bowman (1990). The observations of intense irregularities using the multiple-beam 46.5 MHz MU radar in Japan (Fukao et al., 1991) are particularly interesting. The authors reported periodic uplifting of the midlatitude F-region with high velocities (up to several hundred meters per second) and irregularities down to scale sizes of the radar backscatter length of 3 m. In situ measurements on board satellites and rockets have given great contribution to the present understanding of the ionosphere dynamics. As concerned with long-wave regime, the most interesting feature is the so-called "bubble" upwelling structures ($L > 100$ km; Kelley

* Corresponding author. Tel.: +7-7095-254935; fax: +7-7095-2556040.
E-mail address: oleg@uipe-ras.scgis.ru (O.A. Molchanov).

1474-7065/$ - see front matter © 2004 Published by Elsevier Ltd.
doi:10.1016/j.pce.2003.08.064

et al., 1981; Tsunoda et al., 1982; Tsunoda, 1983). Simultaneous satellite and radar recordings show that these large structures and small-scale irregularities are located in the same area near the equatorial anomaly (EA) of the plasma density, where rather large ion drift velocities $V_i \sim 30$–100 m/s are also registered (see references in Kelley, 1989). Large vertical and longitudinal gradients in the ion concentrations were observed below the F-peak with the retarding potential analyzer on the satellite OGO-6 (Hanson and Sanatani, 1973). The ion density fluctuation measurements have been performed at wavelengths ranging from 70 m to 7 km (McClure et al., 1977; Dyson et al., 1974). Plasma density data from 50 orbits on the Dynamic Explorer II satellite have been analyzed as applied to equatorial F-region irregularities with transverse spatial scales greater than about 1 km (McDaniel and Hysell, 1981). Recent analysis of ion number density measurements made by the retarding potential analyser aboard the AE-E satellite at altitudes above 350 km and below 300 km (Kil and Heelis, 1998) has revealed the existence of longitude variations attributable to F region dynamics. The effect is seen most dramatically in the suppression of occurrence probabilities at altitudes above 350 km in the longitude regions where interhemispheric winds in the magnetic meridian are the largest. There were probe measurements of electrostatic potential fluctuations (Kelley and Mozer, 1972; Dyson et al., 1974) at wavelengths from a few meters to a few kilometers in the low-latitude ionosphere. In particular, vector electric fields in the frequency range (F) from 10 to 500 Hz were measured on the 400 km altitude polar orbiting OV1-17 satellite (Kelley and Mozer, 1972) and Holtet et al. (1977) demonstrated association between F-spread properties and electrostatic noise near low hybrid frequency ($F_{\mathrm{LHR}} \sim 10$–15 KHz). Hoegy et al. (1982) reported on the measurement of fluctuating electric fields on board the DE satellite, where in one example the satellite traversed a series of spread F-bubbles and simultaneously recorded electric field structures with wavelengths of 2–30 m. Recently Aggson et al. (1996) presented electric field data from the San Marco D spacecraft in terms of structure and dynamics of ionospheric plasma (between 500 and 800 km) depletions associated with night side equatorial spread F. They measured two dc electric field components in the zonal flow (westward and eastward) and found bifurcations of these depletions. Rather useful information on multi-scale near-equatorial F-spread turbulence was obtained from the frequency spectra of electron density and electric field fluctuations observed on rockets (see reviews Kelley, 1989, and Hysell, 2000). It is usually supposed that frequency spectrum which is recorded on the moving platform with velocity V_0, represents k-distribution in a manner $\omega' = 2\pi F' \sim kV_0$ (so-called Taylor hypothesis), where F' is the observed frequency of the variations and k is the wave number along the direction of the movement. Thus power spectrum density in a conventional form $\sim (F')^{-b}$ can be converted in the spatial distribution $\sim k^{-b}$ with the same exponent b (fractal index). Jahn and LaBelle (1998) have recently presented the first rocket measurements of equatorial F-spread irregularities at altitudes above 600 km. Power spectra of the electron density fluctuations shows dual-power law behaviour with b indices changed from $b = 1.7$ frequencies below 60 Hz to $b = 5$ at higher frequencies. The electric field fluctuations in their experiment had spectral indices ranging from 3 to 4. Unfortunately such rocket flights are not very regular events. So we will use the same approach in our research but apply it for richer statistics of satellite observations. As far as the authors know, only one paper by Cerisier et al. (1985) was published on the same subject, in which electron density and electric field variations on board the Aureol-3 satellite were analyzed in the frequency range 30–1000 Hz (scales of 10–300 m). They found $b = 1.7$–1.9 for the distribution of both parameters. However they analyzed only one case at $h \sim 600$ km and at a rather high magnetic latitude $\Phi \sim 63°$. Preliminary results of our research on the connection between plasma density-electric field variations and EA from the observation on the satellite IK-24 were recently published by Molchanov et al. (2002). Here we pay main attention to b-statistics from the data obtained on board the Cosmos-900 and IK-24 satellites.

2. Results of Cosmos-900 observation

The satellite Cosmos-900 was operated from 30.03.1977 to 11.09.1979. It had a near-polar orbit (inclination 83° and range of altitude 320–540 km. Plasma density analyzer had a measurement range from 10^1 cm^{-3} to 5×10^{-6} cm^{-3} (see details in Afonin et al., 1999) and sampling rate was 1 per/s, that corresponded to space resolution of about 7 km. First of all we have selected data, which are free from telemetry and equipment malfunction, saturation and so on and which are registered the along orbital segments with magnetic latitudinal interval ±40° around the magnetic equator. As a result we have analyzed 1387 orbital segments during mainly the years of 1977–1978. Examples of registrations are shown in Fig. 1. Two main features of the recordings are a two-hump equatorial anomaly (spatial scale is about 1000 km) and bubbles with scale of hundreds km. In order to reveal smaller-scale variations we construct the variance $V_a = \langle \Delta n^2 \rangle$ and power spectrum density $C_n(F_n)$ for a set of frequencies $F_n = 1/T_n$, $T_n = 2, 3, 4, \ldots, 45$ s, where $\Delta n = n - n_t$ and n_t is running mean in the window ±45 s. In usual assumption (see Introduction) spatial scales $L_n = V_0 T_n$ our averaging window corresponds to ±300 km spatial interval, which is selected to exclude the influence of the EA and large

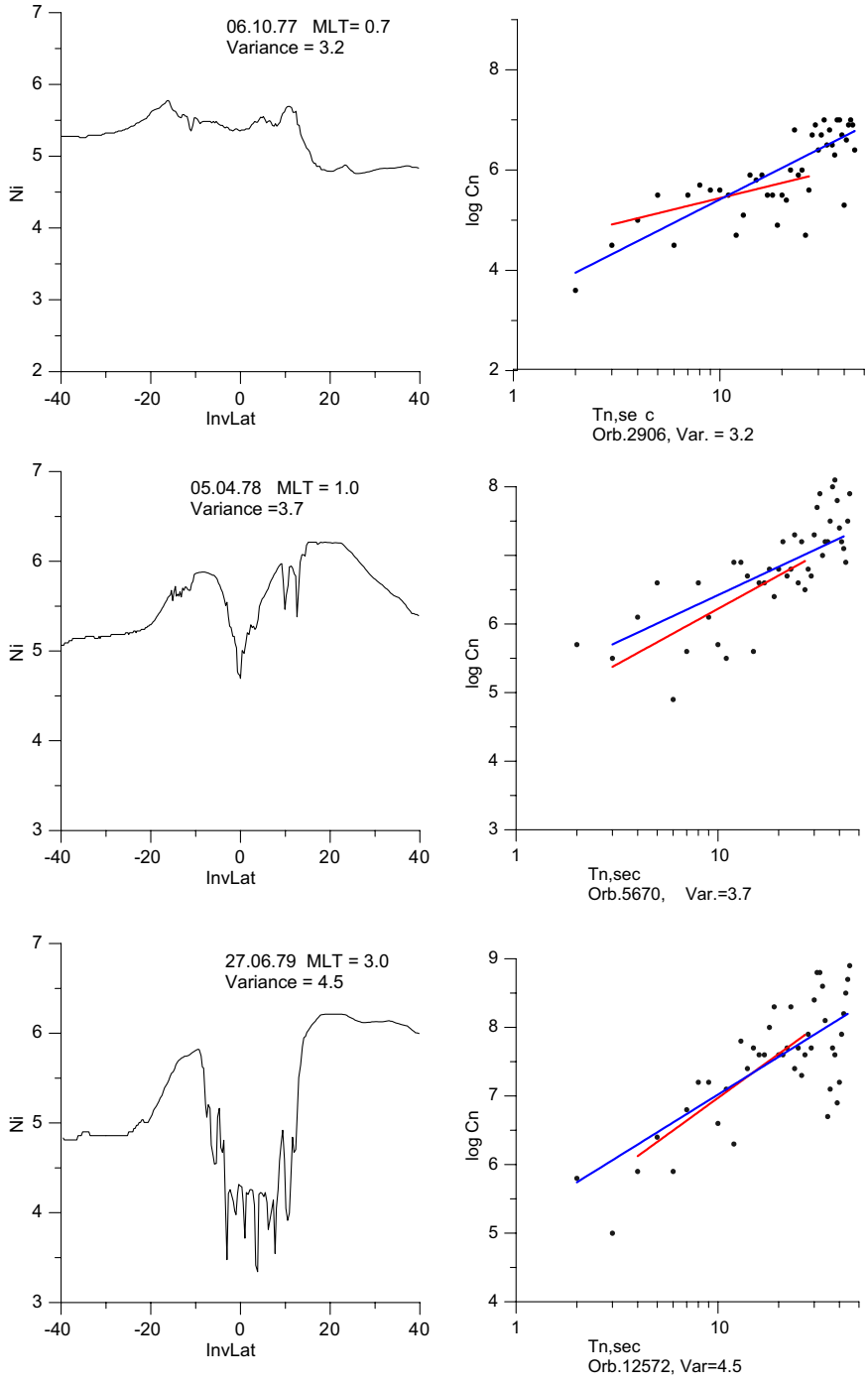

Fig. 1. Examples of the data and *b*-fitting procedure.

bubbles. Then we determine *b*-value as a logarithmic slope of the $C_n(T_n)$ dependence. Examples of *b*-fitting procedure are also presented in Fig. 1. For convenience we plot $V = \log V_a$ as an indicator of the turbulence intensity. Two intervals of the *b*-fitting have been investigated 2–45 and 3–27 s. It is evident that the first interval is better for the data with moderate variance, but the second interval is preferable for the data with large variance. The probable reason is that EA is connected with bubbles and their *k*-distribution is a little bit different from the distribution for small scales. The connection between turbulence intensity and normalized size of EA is demonstrated in Fig. 2. Taking into account that EA-humps are usually ~10–15° in latitude aside of the magnetic equator we assume here normalized EA size as $10(\log N_{\max} - \log N_{\min})/(\log N_{\max} + \log N_{\min})$, where $N_{\max}$ is the maximum value of the electron in the latitudinal interval ±15° (value of the EA

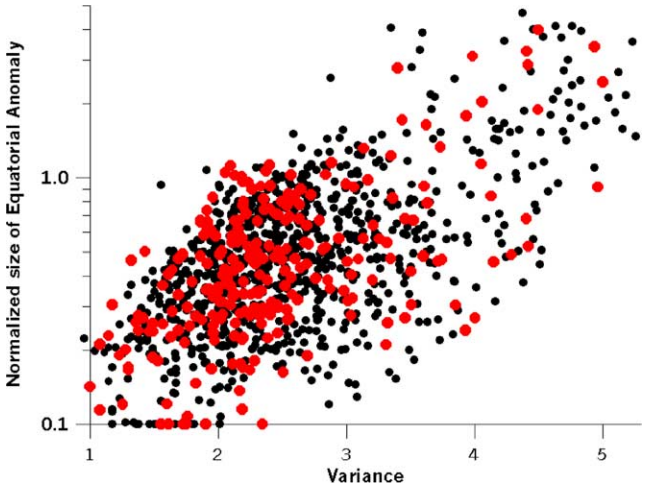

Fig. 2. Dependence of the turbulence intensity (log. variance) on the normalized size of $EA = 10(\log N_{\max} - \log N_{\min})/(\log N_{\max} + \log N_{\min})$, where the maximal and minimal densities are in a margin of ±15° around the magnetic equator.

hump) and $N_{\min}$ is the minimum value in the same interval (as usual at the magnetic equator). Then total b-statistics is shown in Fig. 3a. After it we demonstrate the b-statistics for different and separate sets of data. The first is separation on the seismic orbits, which happened around the time (±7 days) and the position (±15°) of large earthquakes with magnitude $M \geqslant 6$ (EQ hereafter), and nonseismic orbits. It is presented in Fig. 3b. Next is b-statistics in dependence on season (Fig. 4) and local time (Fig. 5). Note that for daytime we have only a few orbits, it is explained by our requirement to exclude the data exceeding saturation level. At last we show the averaged b and V-values in connection with seismicity (Fig. 6). It seems there is a weak tendency for decrease of the b-value and a more regular tendency of decrease in the turbulence intensity in association with selected seismic events.

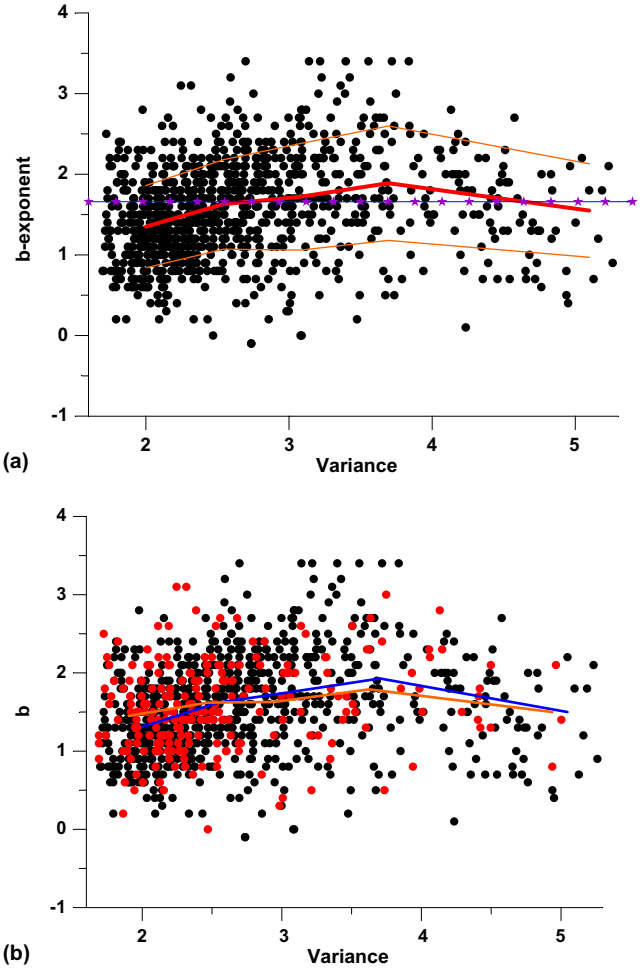

Fig. 3. (a) b-statistics for all the orbits as dependence on the (log) variance; averaged values are shown by solid line, and dispersion margins given by thin lines; (b) the same statistics separately for EQ orbits (red points, averaged values—orange line) and for nonEQ orbits (black points, averaged values—blue line (For interpretation of color in the figure, the reader is referred to the web version of this article.)).

3. Results of IK-24 observation

As mentioned above the comprehensive analysis of the IK-24 data was recently published by Molchanov et al. (2002). The satellite had near-polar inclination ~ 83° and a range of altitudes from 500 to 2500 km. Plasma density analyzer was nearly the same as in Cosmos-900 satellite and ELF-VLF electric field analyzer was described in several papers (e.g. Molchanov et al., 1997). In this paper we produced only analysis of the channels E1 ($F = 10$ KHz) and E2 ($F = 15$ kHz). Examples of the results are shown in Fig. 7. We have found an intensification of electric field turbulence in the near-equatorial region and on the poleward gradients of the EA. While an association of the turbulence with seismicity is not so clear (we found it only for a few cases), a connection of the electric turbulence with EA is doubtless. Fig. 8 presents a relation of the electric field turbulence regions to the position of EA. Then we have tried to estimate the slope of electric field amplitude spectrum by comparison of E1 and E2 values in maxima of both the near-equatorial and shifted anomalies. Using the above-mentioned relation $E(F) \sim F^{-\beta} \sim k^{-\beta}$ it is easy to find:

$$\beta = 2\log(A_1/A_2)/\log(F_2/F_1) + a$$

where A_1 and A_2 are the signal amplitudes after background (noise) reduction and the constant a contains information on the coefficients of amplification and bandwidth. The result is shown in Fig. 9. As can be seen the averaged values of electric field spectrum slope is

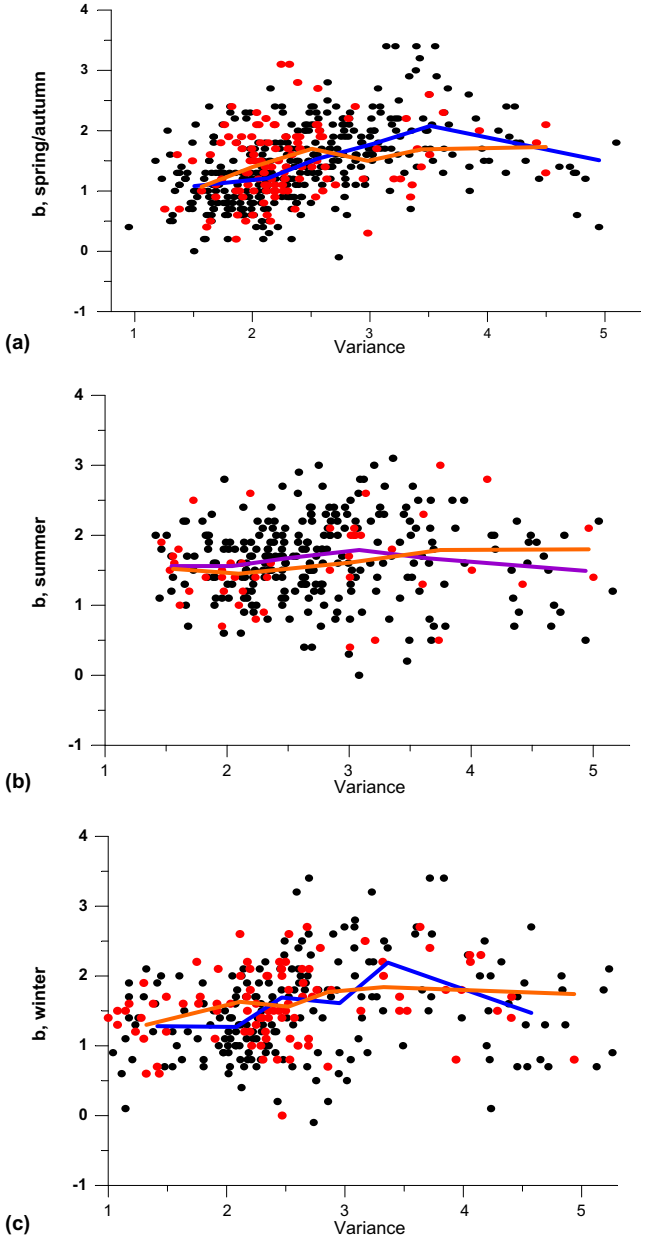

Fig. 4. *b*-statistics separately for different seasons (a) spring-autumn; (b) summer; (c) winter.

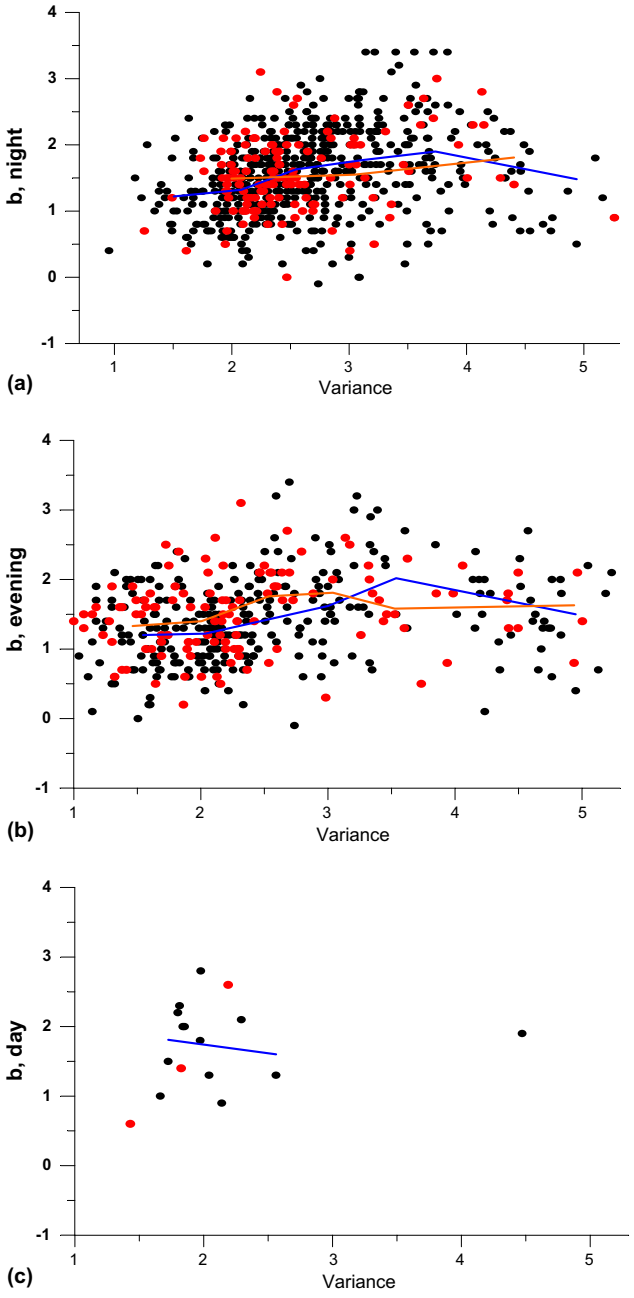

Fig. 5. *b*-statistics for different local times: (a) evening/morning; (b) night; (c) daytime.

$\beta \simeq 3.2$–3.6 and it does not so critically depend on the turbulence type and altitude.

4. Relationship between fractal index β and b

Let us try to find a relationship between the fractal index β for electric field oscillations and the similar index b for density oscillations. We produce it in the so-called hydrodynamic approximation, i.e. assuming that the properties of charged plasma particles $j = \mathrm{e}$ (electrons), i (ions) are described by equations of continuity and motion. Supposing as usual quasi-neutrality ($n_\mathrm{e} = n_\mathrm{i} = n$) and iso-thermal condition ($T_\mathrm{e} = T_\mathrm{i} = T = \mathrm{const}$) the equations are

$$\partial n/\partial t + \nabla(n\mathbf{V})_j = Q_j - \alpha n^2 \quad (1)$$

$$\mathrm{d}\mathbf{V}_j/\mathrm{d}t = (q/m)_j(\mathbf{E} + \mathbf{V}_j \times \mathbf{B}_0) - \nu_j \mathbf{V}_j - C_j^2(\nabla n/n) + g \quad (2)$$

where Q is ionization coefficient, $C_j = (T/m_j)^{1/2}$ is thermal velocity, α is recombination coefficient,

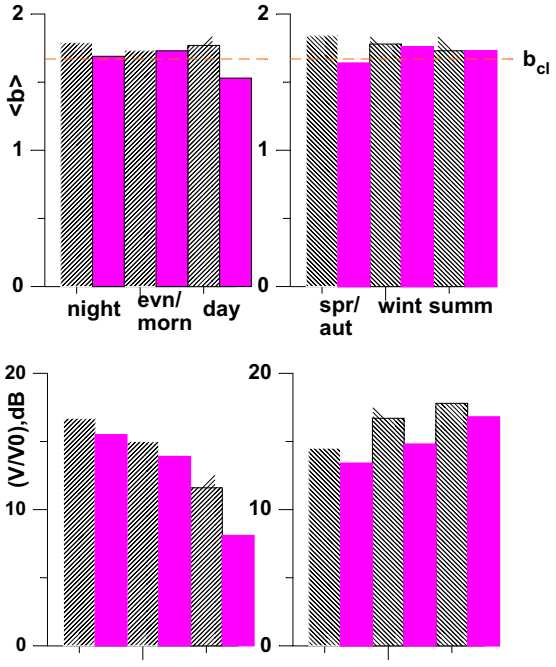

Fig. 6. Averaged b-value in the interval $V = [3, 5]$ (above) and averaged IT intensity (below) for nonseismic orbits (bar with slash lines) and seismic orbits (solid bar) and for different statistics.

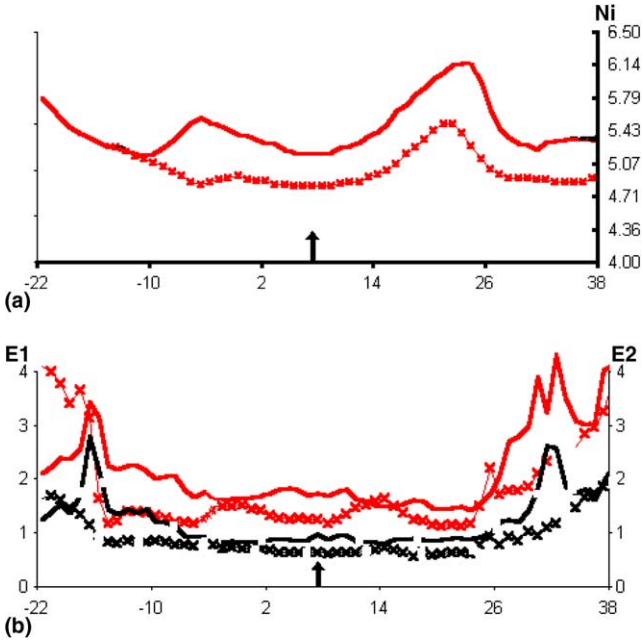

Fig. 7. (a) IK-24 data. Comparison of N_i variations in the latitude interval $\Delta\varphi = \pm 30°$ around the date and epicenter of $M = 7.4$ Philippines Earthquake (15.12.89) for the two orbits: $\Delta t = -8.3$ days, $\Delta\lambda = -10.7°$ (line with crosses) and $\Delta t = +3.6$ days, $\Delta\lambda = +1.3°$ (solid line). Position of EQ (and magnetic equator) is shown by an arrow. (b) The same as above but for electric field variations. Solid line is for 10 kHz channel (E1) and dashed line is for 15 kHz channel (E2).

v_j are collision frequencies and g is acceleration of gravity. Furthermore we use the current continuity

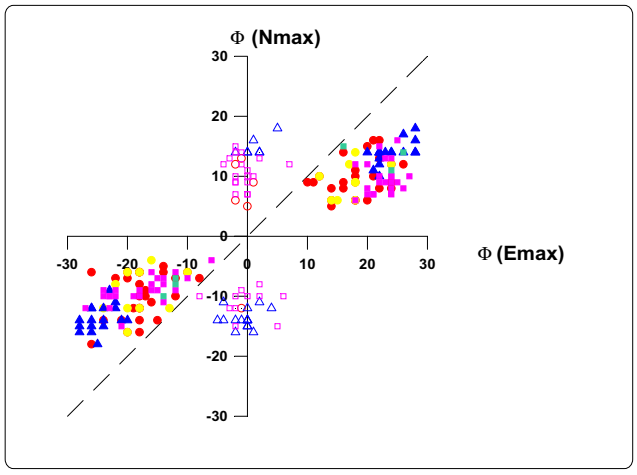

Fig. 8. IK-24 results. Magnetic latitude position of electric field maximums depending on the position of corresponding density maximum in the same orbital segment. Different symbols are used for different seasons (triangles for winter, squares for spring and circles for summer). There are two regions of electric turbulence: the first is near the magnetic equator and second is polar-shifted from the position of EA humps. The latter indicates magnetically-conjugate and its position correlates with the position of EA.

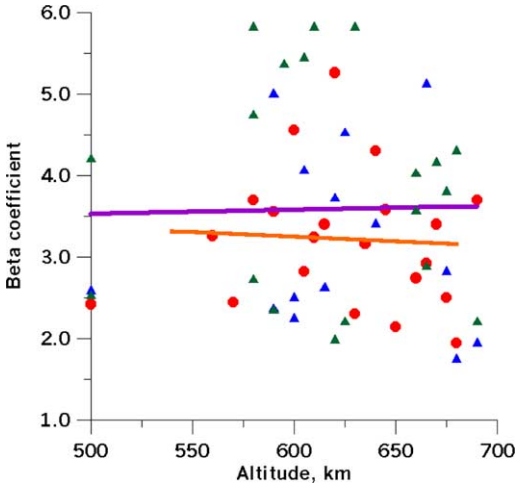

Fig. 9. IK-24 results. Fractal dimension b in dependence on the satellite altitude deduced from the ratio of the electric field power in channels E1 (10 kHz) and E2 (15 kHz, see text). Blue triangles for southward and northward maxima of turbulence in March, 1990, green triangles for the same maxima in winter time (December 1989–January 1990 period), red circles for near-equatorial turbulence in March, 1990. Solid lines are averaged values for near-equatorial electrostatic turbulence (yellow, below) and latitude-shifted turbulence (violet, above) (For interpretation of color in the figure, the reader is referred to the web version of this article.).

equation, which is reduced to the following for $q_i = -q_e = q$,

$$\nabla(n\mathbf{V})_i = \nabla(n\mathbf{V})_e \tag{3}$$

leading to the conclusion:

$$Q_e = Q_i = Q \tag{4}$$

After neglecting the two last right terms in (2), we have traditionally used the following relations:

$$\begin{aligned}
&\mathbf{V}_j(\omega) = \widehat{M}_{j\perp}\mathbf{E}_\perp + M_{jz}\mathbf{E}_z \\
&\widehat{M}_{j\perp} = \frac{1}{B_0(1+X_j^2)}\begin{pmatrix} \pm X_j & 1 \\ -1 & \pm X_j \end{pmatrix} \\
&M_{jz} = \pm 1/B_0 X_j \\
&X_j = (v_j - i\omega)/\omega_{cj} \\
&\omega_{cj} = qB_0/m_j
\end{aligned} \tag{5}$$

Here $\mathbf{B}_0 = B_0\hat{\mathbf{z}}$ and in the whole ionosphere $X_\mathrm{i} \gg X_\mathrm{e}$, therefore $V_{z\mathrm{i}}/V_{z\mathrm{e}} = -X_\mathrm{e}/X_\mathrm{i} = -\beta_\mathrm{e} \sim m_\mathrm{e}/m_\mathrm{i} \ll 1$. Taking it into consideration let us use now the current continuity, Eq. (3), hence:

$$\begin{aligned}
&\nabla_z(nV_{z\mathrm{i}}) = \frac{\beta_\mathrm{e}}{\beta_\mathrm{e}+1}[\nabla_\perp(nV_{\perp\mathrm{e}}) - \nabla_\perp(nV_{\perp\mathrm{i}})] \\
&\partial n/\partial t + \frac{1}{\beta_\mathrm{e}+1}\nabla_\perp(n\mathbf{V})_\mathrm{i} + \frac{\beta_\mathrm{e}}{\beta_\mathrm{e}+1}\nabla_\perp(n\mathbf{V})_\mathrm{e} \\
&\quad \simeq \partial n/\partial t + \nabla_\perp(n\mathbf{V})_\mathrm{i} = Q - \alpha n^2
\end{aligned} \tag{6}$$

Then after linearization and for spectral components:

$$\begin{aligned}
&n = n_0 + \delta n \quad \mathbf{V}_{\perp\mathrm{i}} = \mathbf{V}_0 + \mathbf{v}_{\perp\mathrm{i}} \quad Q = Q_0 + \Delta Q \\
&\delta n_k/n_0 = (\mathbf{k}\mathbf{v}_{\perp\mathrm{i}} + i\Delta Q/n_0)/(\omega - \mathbf{k}\mathbf{V}_0 + i\omega_r) \\
&\omega_r = 2\alpha n_0
\end{aligned} \tag{7}$$

As concerned with Q_0 at nighttime it is mainly due to flux of the hot electrons $J = n_\mathrm{h}V_\mathrm{h}$. This flux produces ionization in the layer Δz, thus

$$\begin{aligned}
&Q_0 = J_\mathrm{h}/\Delta z = j_0/(q\Delta z) \quad j_0 = qJ_\mathrm{h} = qn_\mathrm{h}V_\mathrm{h} \\
&Q_0 = \alpha n_{0\mathrm{i}}^2 \quad n_\mathrm{h}/n_{0\mathrm{i}} = \omega_r\Delta z/(2V_\mathrm{h}) \\
&\Delta z = j_0/(\alpha q n_{0\mathrm{i}}^2) \sim 10^{20} j_0/[n_{0\mathrm{i}}^2(\mathrm{cm}^{-3})]
\end{aligned} \tag{8}$$

Now we are going to estimate the input from the impact ionization and we need in a model of the alternative source ΔQ supposing for simplicity some modulation by the Alfven wave in the magnetosphere.

(A) The natural model where Alfven waves modulate the flux velocity, i.e.

$$\begin{aligned}
&V_\mathrm{h} = V_{\mathrm{h}0} + \Delta V_z \quad \Delta Q = n_\mathrm{h}\Delta V_z/\Delta z = (n_\mathrm{h}/n_{0m})j_{zA}/(q\Delta z) \\
&j_{zA} = ik\sigma_{z\mathrm{e}}(\partial E_{xm}/\partial z)(i\omega\mu\sigma_{z\mathrm{e}} - k^2) \simeq ikE_{xm}/(\mu C_{Am}) \\
&i\Delta Q/n_{0\mathrm{i}} = -(n_\mathrm{h}/n_{0\mathrm{i}})[kC_{Am}/(\omega_{ci,m}\Delta z)](E_{xm}/B_{0m})
\end{aligned} \tag{9}$$

Using the following relation from (5),

$$\begin{aligned}
&\mathbf{k}\mathbf{v}_{\perp i} = kE_{xi}A(X_\mathrm{i})/B_0 \\
&A(X_\mathrm{i}) = \langle X_\mathrm{i}/(1+X_\mathrm{i}^2)\rangle
\end{aligned} \tag{10}$$

we have

$$\begin{aligned}
&\mathbf{k}\mathbf{v}_{\perp\mathrm{i}} + i\Delta Q/n_0 = \mathbf{k}\mathbf{v}_{\perp i}(1+D) \\
&D = -\frac{n_\mathrm{h}}{n_{0\mathrm{i}}}\frac{C_{Am}}{A\omega_{ci,m}\Delta z}\frac{B_{0\mathrm{i}}}{B_{0m}}\frac{E_{xm}}{E_{xi}}
\end{aligned} \tag{11}$$

In the upper ionosphere $A \simeq X_\mathrm{i} \simeq -i\omega/\omega_{ci}$ and $D = i(\omega_r/\omega)(C_{Am}/2V_\mathrm{h})(E_{xm}/E_{xi})$, but in the middle ionosphere ($h \sim 100$–200 km) $A \simeq 1$ and $D = -(\omega_r/\omega_{ci,m})(C_{Am}/2V_\mathrm{h})(E_{xm}/E_{xi})$. It is easy to find that in both cases $|D| \ll 1$.

(B) Lysak (1991) and Pokhotelov et al. (2000) suggested other model:

$$\Delta Q = \frac{j_{zA}}{q\Delta z} \tag{12}$$

We estimate it for the turbulence inside the ionosphere, $A \sim 1$, hence:

$$\begin{aligned}
D &= -\frac{n_{0m}}{n_{0\mathrm{i}}}\frac{C_{Am}}{\omega_{ci,m}\Delta z}\frac{B_{0\mathrm{i}}}{B_{0m}}\frac{E_{xm}}{E_{xi}} \\
&= -\frac{C_{Am}^2}{C_{Ai}\omega_{ci,m}\Delta z}\frac{n_{0m}}{n_{0i}}\frac{B_{0\mathrm{i}}}{B_{0m}}\frac{b_{xm}}{b_{xi}} \ll 1
\end{aligned} \tag{13}$$

As a result, using (7) we can write the connection between density and electric field turbulence, which are observed on the moving satellite with velocity V_0 as follows:

$$\begin{aligned}
&(\delta n_k/n_0)^2 = T(\omega_k - \omega', k)E_k^2 \\
&T = k^2/\left|(\omega_k - \omega')^2\left(1 + X_\mathrm{i}'^2\right)\right| \\
&\omega' = kV_0 \\
&X_i' = \left[\nu_\mathrm{i} - i\left(\omega_k - \omega'\right)\right]/\omega_{ci}
\end{aligned} \tag{14}$$

where isotropic turbulence is supposed: $\langle E_x^2\rangle = \langle E_y^2\rangle$ and it is evident that ω' is the frequency of observed variations, if group velocity V_g of the turbulent waves is small, i.e.:

$$V_\mathrm{g} = \partial\omega_k/\partial k \ll V_0 \tag{15}$$

There are two main possibilities. Taking into consideration that $\nu_\mathrm{i} \ll \omega_{ci}$ at the satellite heights ($h > 350$ km) the first possibility is:

$$V_\mathrm{ph} = \omega_k/k \ll V_0 \quad \omega_k \ll \omega' \tag{16}$$

In this case of small phase velocity

$$T = (\omega_{ci}^2/V_0^2B_0^2)/(\omega_{ci}^2 + k^2V_0^2) \tag{17}$$

and $(\delta n_k/n_0)^2 \simeq E_k^2$ if $\omega' \leqslant \omega_{ci}$. It means the k-distribution of the density and electric field variations is the same. Here $\omega_{ci} = 2\pi F_{ci}$ is an effective ion cyclotron frequency, which varied from the value $F_{ci} \sim 40$ Hz (daytime near the equatorial F-layer, main ion constituent O^+) to $F_{ci} \sim 500$ Hz (night-time, polar region, main ion H^+). So we can expect that similarity of the density and electric field k-spectrum could be kept up to $F' \sim 50$–100 Hz in the near-equatorial ionosphere at the altitudes 500–700 km. Probably it is a case of the Aureol-3 data. But if $\omega' \geqslant \omega_{ci}$ then $(\delta n_k/n_0)^2 \simeq E_k^2/k^2$ and the expected spectrum of the density is sharper than that for electric field turbulence, $b \simeq \beta + 2$. However, for our IK-24 observation just an opposite case is probable, when:

$$\omega_k \simeq \omega_\mathrm{res} \gg \omega' \gg \omega_{ci} \quad T \simeq k^2\omega_{ci}^2/(\omega_\mathrm{res}^4B_0^2) \tag{18}$$

where ω_{res} is frequency of electrostatic oscillation above low hybrid resonance angular frequency ω_{LHR} ($\omega_{LHR} < \omega_{res} < \omega_{ce}$). In this case $(\delta n_k/n_0)^2 \simeq k^2 E_k^2$ and

$$b \simeq \beta - 2 \tag{19}$$

It is easy to find that the condition (15) in our case can be true because of:

$$\begin{aligned} &k = \omega'/V_0 \leqslant 10\ \mathrm{m}^{-1} \\ &\omega_k = \omega_{res}/(1 + k_0^2/ak^2)^{1/2} \simeq \omega_{res}(1 - k_0^2/2ak^2) \\ &k_0 = \omega_{ce}/c \simeq 10^{-2}\ \mathrm{m}^{-1} \\ &\partial\omega_k/\partial k \simeq C_A(k_0/k))^3 \ll V_0 \end{aligned} \tag{20}$$

5. Discussion

Let us summarize the results of satellite observations on the turbulence slope in the following table:

Satellite	Type of turbulence	Frequency (Hz)	H (km)	Scale	$\beta(E)$	$b(n)$
Cosmos-900	n_k	0.02–0.5	320–540	15–300 km		1.3–2.0
Aureol-3	n_k, E_k	10–500	500–700	15–700 m	1.7–1.9	1.7–1.9
IK-24	E_k, (n_k)	10–15	500–700	0.5–0.7 m	3.2–3.6	1.2–1.6

Similarity of the density slope in the large scope of scales suggests a possibility of the ionospheric turbulence development similar to the classic Kolmogorov's turbulence (Kolmogorov, 1941). Note that the classic value of $b = 5/3$ is shown in Fig. 3a in comparison with our averaged observational values. We will try to discuss this possibility in a future paper. We will suppose that atmospheric gravity waves (AGW) are not "seeding" but forcing reason of the nonlinear turbulence development. On this way a connection of the EA and smaller scale turbulence means that the turbulence has largest scale (like a scale of an "obstacle" in the laminar flow in classic theory). As concerned with our assumption on existence of the electrostatic oscillations above ω_{LHR} it was extensively discussed in several papers (Costa and Kelley, 1978; Sperling and Goldman, 1980). At last a connection with seismicity can also be explained by change of the AGW forcing during the processes of the EQ preparation, as it is discussed in the paper by Mareev et al. (2002).

Acknowledgements

This research was partially supported by ISTC under Grant 1121 and by Commision of the EU (grant No. INTAS-01-0456). An author (O.A. Molchanov) is thankful for the support from International Space Science Institute (ISSI) at Bern, Switzerland within the project "Earthquake influence of the ionosphere as evident from satellite density-electric field data".

References

Aggson, T.L., Laakso, H., Maynard, N.C., Pfaff, R.F., 1996. In situ observations of bifurcations of equatorial bubbles. J. Geophys. Res. 101, 5125–5138.

Afonin, V.V., Molchanov, O.A., Kodama, T., Hayakawa, M., Akentieva, O.A., 1999. Ionospheric response to long seismic influence: Search for reliable result from satellite observations. In: Hayakawa, M. (Ed.), Atmospheric and Ionospheric Electromagnetic Phenomena Associated with Earthquakes. Terra Sci. Publ. Comp., Tokyo, pp. 597–618.

Basu, Su., Basu, Sa., Ganguly, S., Clobuchar, J.A., 1981. Generation of kilometer scale irregularities during the midnight collapse at Arecibo. J. Geophys. Res. 86, 7607.

Bowman, G.G., 1990. A review of some recent work on midlatitude spread F occurrence as detected by ionosondes. J. Geomagn. Geoelectr. 42, 109.

Cerisier, J.C., Berthelier, J.J., Beghin, C., 1985. Unstable density gradients in the high-latitude ionosphere. Radio Sci. 20, 755–761.

Costa, C.S., Kelley, M.C., 1978. Linear theory for the collisionless drift wave instability with wavelengths near the ion gyroradius. J. Geophys. Res. 83, 4365–4368.

Dyson, P.L., McClure, J.P., Hanson, W.B., 1974. In situ measurements of the spectral characteristics of F region ionospheric irregularities. J. Geophys. Res. 79, 1497–1502.

Fejer, B.G., Kelley, M.C., 1980. Ionospheric irregularities. Rev. Geophys. 18, 401–450.

Fejer, B.G., 1997. The electrodynamics of the low-latitude ionosphere: Recent results and future challenges. J. Atmos. Solar-Terr. Phys. 59, 1456–1482.

Fukao, S., Kelley, M.C., Shirakawa, T., Takami, T., Yumamoto, M., Tsuda, T., Kato, S., 1991. Turbulent upwelling of the mid-latitude ionosphere, 1, Observation results by the MU radar. J. Geophys. Res. 96, 3725–3746.

Hanson, W.B., Sanatani, S., 1973. Large Ni gradients below the equatorial F peak. J. Geophys. Res. 78, 1167–1173.

Hoegy, W.R., Curtis, S.A., Brace, L.H., Maynard, N.C., Heelis, R.A., 1982. Dynamic explorer observations of equatorial spread F: Evidence for drift waves. Geophys. Res. Lett. 9, 993–996.

Holtet, J.A., Maynard, N.C., Heppner, J.P., 1977. Variational electric fields at low latitudes and their relation to spread-F and plasma irregularities. J. Atmos. Terr. Phys. 39, 247–262.

Hysell, D.L., 2000. An overview and synthesis of plasma irregularities in equatorial spread F. J. Atmos. Terr. Phys. 62, 1037–1056.

Jahn, J.M., LaBelle, J., 1998. Rocket measurements of high-altitude spread F irregularities at the magnetic dip equator. J. Geophys. Res. 103, 23,427–23,441.

Kelley, M.C., Mozer, F.S., 1972. A satellite survey of vector electric fields in the ionosphere at frequencies of 10 to 500 Hertz, 3, Low-frequency equatorial emissions and their relationship to ionospheric turbulence. J. Geophys. Res. 77, 4174.

Kelley, M.C., Larson, M.F., La Hoz, C., McClure, J.P., 1981. Gravity wave initiation of equatorial spread F: A case study. J. Geophys. Res. 86, 9087–9100.

Kelley, M.C., 1985. Equatorial spread F: recent results and outstanding problems. J. Atmos. Terr. Phys. 47, 745–752.

Kelley, M.C., 1989. The Earth's Ionosphere: Plasma Physics and Electrodynamics, Int. Geophys. Ser., 43, Academic Press, San Diego, California.

Kil, H., Heelis, R.A., 1998. Global distribution of density irregularities in the equatorial ionosphere. J. Geophys. Res. 103, 407–417.

Kolmogorov, A.N., 1941. The local structure of turbulence in incompressible viscous fluids for very high Reynolds numbers. Dokl. Acad. Nauk SSSR 30, 301–304.

Lysak, R.L., 1991. Feedback instability of the ionospheric resonant cavity. J. Geophys. Res. 96, 1553.

Mareev, E.A., Iudin, D.I., Molchanov, O.A., 2002. Mosaic source of internal gravity waves associated with seismic activity. In: Hayakawa, M., Molchanov, O.A. (Eds.), Seismo-Electromagnetics (Lithosphere–Atmosphere–Ionosphere Coupling). TERRUPUB, Tokyo, pp. 335–343.

McClure, J.P., Hanson, W.B., Hoffman, J.H., 1977. Plasma bubbles and irregularities in the equatorial ionosphere. J. Geophys. Res. 82, 2650–2656.

McDaniel, R.D., Hysell, D.L., 1981. Models and DE II observations of inertial-regime irregularities in equatorial spread F. J. Geophys. Res. 86, 9087–9100.

Molchanov, O.A., Mogilevsky, M.M., Afonin, V.V., Klos, Z., Hayakawa, M., Shima, N., 1997. Nonlinear ELF-VLF effects observed on ACTIVNY satellite. In: Hada, T., Matsumoto, H. (Eds.), Nonlinear Waves and Chaos in Space Plasmas. Terra Sci. Publ. Comp., Tokyo, pp. 337–358. chapter 10.

Molchanov, O.A., Hayakawa, M., Afonin, V.V., Akentieva, O.A., Mareev, E.A., 2002. Possible influence of seismicity by gravity waves on ionospheric equatorial anomaly from data of IK-24 satellite, 1. Search for idea of seismo-ionosphere coupling; 2. Equatorial anomaly and small-scale ionospheric turbulence. In: Hayakawa, M., Molchanov, O.A. (Eds.), Seismo-Electromagnetics (Lithosphere–Atmosphere–Ionosphere Coupling). TERRUPUB, Tokyo, pp. 275–297.

Pokhotelov, O.A., Pokhotelov, D.O., Streltsov, A., Khruschev, V., Parrot, M., 2000. Dispersive ionospheric Alfven resonator. J. Geophys. Res. 105, 7737.

Sperling, J.L., Goldman, S.R., 1980. Electron collisional effects on lower hybrid drift instabilities in the ionosphere. J. Geophys. Res. 85, 3494–3498.

Tsunoda, R.T., Livingstone, R.G., McClure, J.P., Hanson, W.B., 1982. Equatorial plasma bubbles: vertically elongated wedges from the bottomside F layer. J. Geophys. Res. 87, 9171–9180.

Tsunoda, R.T., 1983. On the generation and growth of equatorial backscatter plumes, 2, Structuring of the west walls of upwellings. J. Geophys. Res. 88, 4869–4874.